Chinese Chemical Letters 36 (2025) 109819

Contents lists available at ScienceDirect

Chinese Chemical Letters

journal homepage: www.elsevier.com/locate/cclet

An ionic liquid functionalized sericin hydrogel for drug-resistant bacteria-infected diabetic wound healing

Jiajia Wang[a,b,1], XinXin Ge[c,1], Yajing Xiang[c], Xiaoliang Qi[a,*], Ying Li[b], Hangbin Xu[c], Erya Cai[c], Chaofan Zhang[a,b], Yulong Lan[d], Xiaojing Chen[d], Yizuo Shi[d], Zhangping Li[e,*], Jianliang Shen[a,d,*]

[a] National Engineering Research Center of Ophthalmology and Optometry, Eye Hospital, Wenzhou Medical University, Wenzhou 325027, China
[b] School of Chemical Engineering, Nanjing University of Science & Technology, Nanjing 210094, China
[c] School & Hospital of Stomatology, Wenzhou Medical University, Wenzhou 325027, China
[d] Zhejiang Engineering Research Center for Tissue Repair Materials, Wenzhou Institute, University of Chinese Academy of Sciences, Wenzhou 325001, China
[e] The Quzhou Affiliated Hospital of Wenzhou Medical University, Quzhou People's Hospital, Quzhou 324000, China

ARTICLE INFO

Article history:
Received 16 January 2024
Revised 21 March 2024
Accepted 22 March 2024
Available online 23 March 2024

Keywords:
Sericin
Ionic liquids
Hydrogels
Methicillin-resistant *Staphylococcus aureus* infection
Diabetic wound healing

ABSTRACT

Diabetic wound healing is often complicated due to bacterial infections that intensify inflammation. Employing hydrogel dressings with inherent antibacterial properties can significantly reduce reliance on antibiotics for treating infected wounds in diabetics. Traditional hydrogels typically rely on the infiltration of bacteria into their porous structure to manifest antibacterial effects. However, this infiltration process is not only prolonged but can also exacerbate inflammation, further delaying the healing of the wound. Thus, promptly capturing and eliminating bacteria is crucial for enhancing the antibacterial efficiency of the hydrogel. In this context, we present a multifunctional hydrogel dressing, termed SIP, designed to tackle drug-resistant bacterial infections in diabetic wounds. This dressing integrates ionic liquid functional groups into a sericin-based matrix: phenylboronic acid for the immobilization of bacteria and imidazole for their subsequent annihilation. Expectedly, the SIP system demonstrates potent antibacterial activity against methicillin-resistant *Staphylococcus aureus*, verified through *in vitro* and *in vivo* experiments. As a result, SIP emerges as a promising candidate in the realm of hydrogel dressings with innate antibacterial properties, showcasing considerable potential for addressing diabetic wounds plagued by drug-resistant bacterial infections.

Diabetes mellitus poses a significant threat to public health, resulting in substantial productivity losses and financial burdens, with healthcare costs in the United States surpassing $327 billion each year [1]. These expenses are projected to escalate by 1 billion annually, contributing to an increase in the number of years individuals live with disabilities. In the United States, around 30 million individuals are affected by diabetes, and a significant complication they encounter includes diabetic foot ulcers [2]. These ulcers are prevalent in 15% to 25% of individuals with diabetes and can lead to amputations if not treated properly [3]. Although there are established protocols for wound care management, challenges persist due to the multifactorial nature of the condition, specific patient circumstances, stringent regulatory and market entry barriers, the integration of new biologics-based therapies, and ensuring adequate access to medical care [4,5]. The onset of infection further complicates the management of diabetic wounds, negatively impacting the patient's overall health status [6]. For instance, the likelihood of lower limb amputation in patients with infected diabetic foot ulcers (DFUs) is 50% higher compared to those with non-infected ulcers [7,8]. Considering these various challenges, there is a pressing need to identify and develop therapeutic alternatives that are safer, more effective, and more cost-efficient for handling infected diabetic wounds [9,10].

Currently, antibiotics are the primary approach for addressing bacterial infections in the healing process of diabetic wounds [11,12]. However, the widespread and prolonged use of antibiotics has contributed to a rise in bacterial resistance, leading to the development of antibiotic-resistant variants like methicillin-resistant *Staphylococcus aureus* (MRSA) [13]. Due to MRSA's robust nature, there is a requirement for higher and more potent antibiotic doses, increasing the risk of negative drug reactions [14,15]. As a re-

* Corresponding authors.
E-mail addresses: xiaoliangqi90@gmail.com (X. Qi), wzlizhangping@126.com (Z. Li), sjl1@wmu.edu.cn, shenjl@wiucas.ac.cn (J. Shen).
[1] These authors contributed equally to this work.

https://doi.org/10.1016/j.cclet.2024.109819
1001-8417/

sult, conventional antibiotic methods are becoming less effective against MRSA-related diabetic wound infections, highlighting the critical need for alternative treatments in the medical field [16,17]. A substantial amount of research has been dedicated to developing dressings capable of combating MRSA-infected diabetic wound infections effectively. Among various dressing options, hydrogels are particularly notable due to their inherent antibacterial properties, extensive bactericidal capacities, adjustable physical features, and excellent biocompatibility [18,19]. The moisture-laden composition of hydrogels helps maintain optimal hydration levels in the wound, reducing the likelihood of scar tissue formation [20]. In addition, hydrogels are proficient at absorbing wound exudate and provide a robust barrier against microbial penetration [21,22]. These characteristics make hydrogel-based dressings a promising option for treating diabetic wounds compromised by infection.

Sericin (Ser), a hydrophilic protein derived from silkworm cocoons, has recently garnered substantial attention for its potential in hydrogel wound dressing fabrication. This is attributed to its biocompatibility, biodegradability, and properties that include anti-aging, anti-coagulation, and anti-tyrosinase effects. Ser is particularly notable for its ability to promote the growth and proliferation of fibroblasts and keratinocytes. When modified with methacrylic anhydride (MA), Ser transforms into methacrylic anhydride sericin (SerMA), exhibiting remarkable properties such as injectability, adhesion, and biocompatibility. These characteristics highlight the potential of SerMA in facilitating wound healing. Nevertheless, conventional SerMA hydrogels face limitations in treating wounds with bacterial infections, primarily due to their ineffectiveness in capturing and neutralizing bacteria. This is because SerMA lacks potent bacterial trapping and killing sites, making it difficult for bacteria to access and penetrate the hydrogel's porous matrix [23]. To enhance the antibacterial efficiency of SerMA hydrogel, ensuring efficient bacterial capture and elimination becomes imperative. In a novel approach, the introduction of phenylboronic acid groups has shown potential in creating reversible covalent bonds with *cis*-diol molecules commonly found in glycoproteins on bacterial surfaces. This mechanism is progressively becoming a popular choice for bacterial detection. Furthermore, the addition of positively charged imidazole groups provides the means to interact electrostatically with the negatively charged bacterial membranes. This interaction disrupts the bacterial membranes' permeability and hydrodynamics, resulting in an antibacterial effect. Therefore, we suggest that by integrating phenylboronic acid groups for bacterial trapping and imidazole groups for bacterial destruction into SerMA hydrogel dressings, we could establish a promising strategy for attaining robust antibacterial activity.

In this study, we investigate an innovative strategy to treat bacterially infected diabetic wounds by integrating functional groups into a SerMA hydrogel matrix that can entrap (using phenylboronic acid) and annihilate bacteria (using imidazole). As depicted in Scheme 1, a protective hydrogel barrier named SIP forms over the wound site *via* a straightforward local injection followed by subsequent photoinitiation. The SIP barrier efficiently captures and eradicates bacteria, contributing to decreased inflammation and aiding the wound's transition from an inflammatory state to a proliferative phase. We carried out a thorough evaluation of the SIP hydrogel system in its injectable form, including assessments both *in vitro* and *in vivo*. For *in vitro* evaluations, we explored a variety of physicochemical characteristics such as swelling behavior, capacity to retain water, structural morphology, and biocompatibility, along with the ability to capture bacteria and exhibit antibacterial properties. Diabetic rat models served for *in vivo* evaluations of wound healing capabilities, with a focus on wounds situated on the back and feet. In conclusion, our results pave the way for new methods in the management and treatment of bacterial infections in diabetic patients.

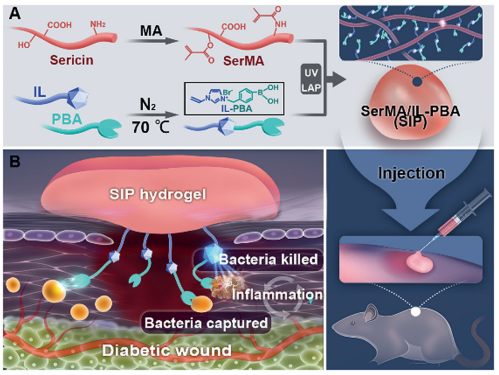

Scheme 1. Formulation and application of SIP hydrogel for hastening wound healing in diabetic rats infected with drug-resistant bacteria. (A) SIP hydrogel synthesis pathway. (B) Methods through which SIP hydrogel promotes recovery in wound healing.

The samples' functional property changes were examined using proton nuclear magnetic resonance (^{1}H NMR) and Fourier transform infrared (FT-IR) techniques. In the ^{1}H NMR spectrum of imidazole-phenylboronic acid (IL-PBA), the resonance peaks of the carbon-carbon double bond, characteristic of IL, were prominent at 7.33, 6.00, and 5.43 ppm. Additionally, three distinct peaks at 7.97, 8.26, and 9.70 ppm aligned with IL's characteristic peaks. The PBA's characteristic peaks corresponded at 8.09 ppm (–OH) and 5.50 ppm ($-CH_2$), along with benzene ring peaks at 7.43 and 7.84 ppm. The detection of characteristic groups from both IL and PBA suggests the successful creation of IL-PBA, as depicted in Figs. 1A and B.

To examine the changes in functional groups after modifying Ser, the study utilized both NMR and FT-IR spectroscopic techniques. A significant shift was noted in the NMR spectra when Ser and its modified counterpart, SerMA, were compared. The ^{1}H NMR spectrum of SerMA displayed distinct resonance peaks indicative of carbon-carbon double bonds at 5.57 and 5.97 ppm (Fig. 1C). This evidence supports the effective integration of glycidyl methacrylate into Ser. Moreover, the appearance of a methyl group signal at 1.76 ppm further confirms the successful formation of SerMA.

FT-IR spectroscopy was employed to analyze the chemical composition of SIP hydrogels, as illustrated in Fig. 1D. The FT-IR spectra revealed distinct Ser peaks corresponding to amide I, II, and III at 1649, 1514, and 1231 cm^{-1}. These characteristic peaks were similarly identified in the FT-IR analyses of both SIP0 and SIP2 hydrogels, suggesting that Ser's secondary structure in these hydrogels was an unordered conformation. PBA's primary characteristic peaks at 1350 cm^{-1} (B–O), 1407 cm^{-1} (C–B), and 1613 cm^{-1} were identified as aromatic ring skeleton vibration peaks. In the case of IL, stretching vibrations of imidazolium rings were noted at 960 cm^{-1} (=C–H), 1502 cm^{-1} (C–N), and 1651 cm^{-1} (C=N). Each of these characteristic peaks, including those of IL-PBA, showed a discernible shift. Collectively, these findings validate the successful synthesis of the SIP hydrogels.

Next, the formation of SIP hydrogels was observed on a macroscopic scale, as illustrated in Fig. 1E. Following this, scanning electron microscopy (SEM) was employed to investigate the surface morphology and microscale porosity of the lyophilized SIP hydrogels (Figs. 1F and G) [24]. SIP0 (devoid of IL-PBA) and SIP2 (with 0.6 mg/mL IL-PBA) hydrogels displayed a porous, three-dimensional lattice configuration conducive to the absorption of wound exudate and the growth of cells [25]. Furthermore, the integration of IL-PBA into the SerMA hydrogel led to a decrease in the average pore diameter to 35.7 ± 6 μm (Fig. 1F), a contrast to the SIP0's pore dimension of 44.9 ± 7 μm (Fig. 1G). This reduction in pore size is

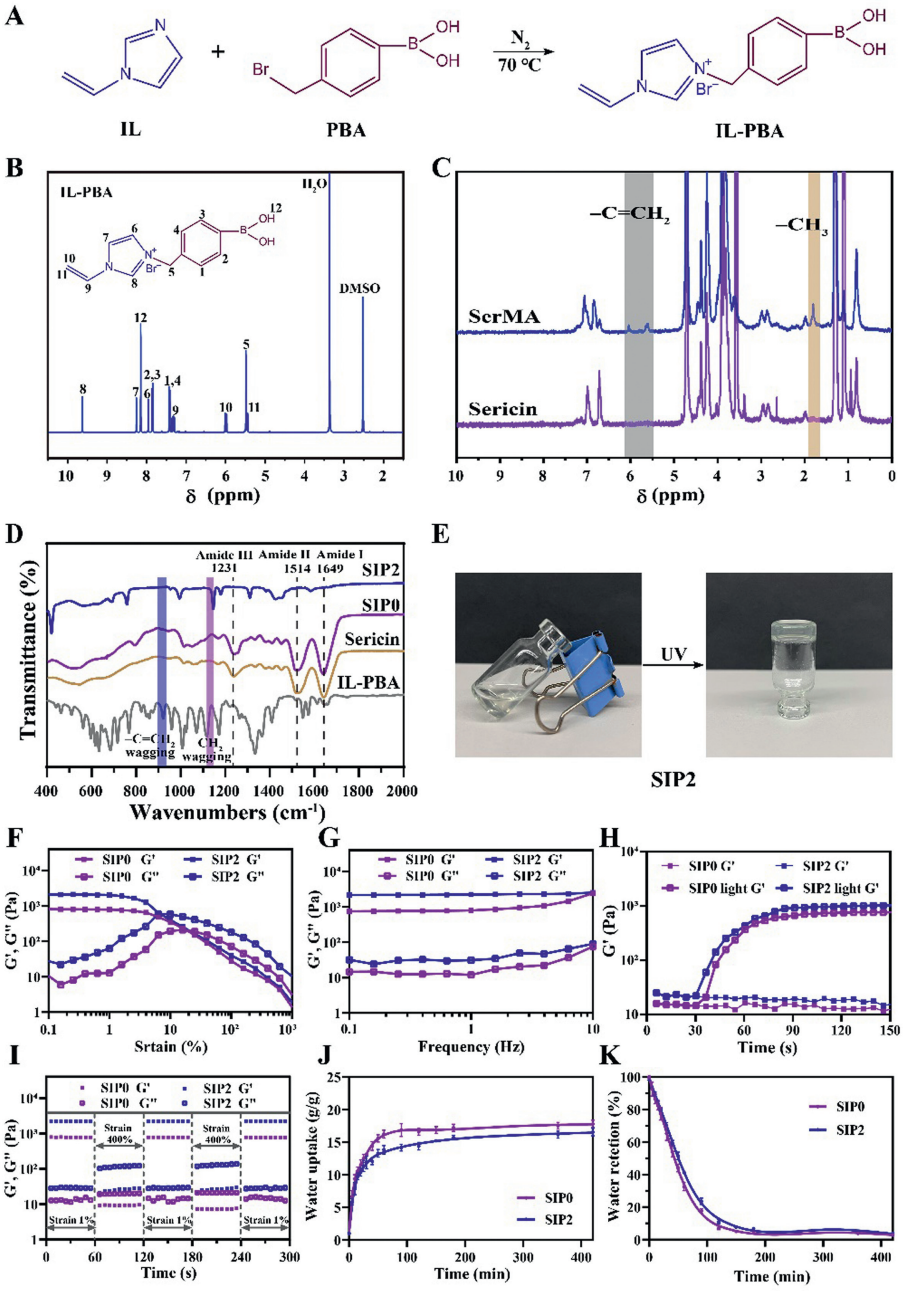

Fig. 1. Physicochemical traits of SIP hydrogels. (A) Schematic representing IL-PBA synthesis. (B) ^{1}H NMR spectral presentation in DMSO for IL-PBA. (C) ^{1}H NMR spectral profiles of SerMA and Ser. (D) IL-PBA, Ser, SIP0, and SIP2 FT-IR spectral analysis. (E) Macroscopic observation of SIP hydrogel formation. (F) Rheological analysis over time, focusing on the photo-induced mechanical strengthening of SIP hydrogels. (G) Study of SIP hydrogels' rheological behavior dependent on frequency at a 1% strain. (H) Analysis of changes in SIP hydrogels' rheological properties with varying strains at a frequency of 0.1 Hz. (I) Outcomes of step-strain testing on SIP hydrogels, contrasting the effects of 1% and 400% strains at a steady 0.1 Hz frequency. (J, K) Assessments of SIP hydrogels' swelling (J) and moisture retention abilities (K). Error bars denote the mean ± standard deviation (SD) ($n = 3$).

attributed to enhance cross-linking brought about by the introduction of ionic monomers [26].

Subsequently, the SIP hydrogels' rheological characteristics were thoroughly assessed. Hydrogel dressings typically need to show robust mechanical strength and flexibility to conform to the dynamic, intricate wound microenvironments. As shown in Fig. 1F, exposure to ultraviolet light significantly bolstered the gel's mechanical attributes, notably increasing the G' roughly tenfold, from 102 Pa to 1013 Pa. Then, oscillatory frequency tests between 0.1 Hz and 10 Hz were conducted to explore the hydrogels' rheological behaviors dependent on frequency, as illustrated in Fig. 1G. Throughout these frequency ranges, the hydrogels displayed a consistently higher G' compared to G'', indicating their primarily elastic characteristics. Additionally, strain scan tests were performed to determine the hydrogels' linear viscoelastic range (Fig. 1H). Specifically, the SIP2 hydrogel showed a transition point near 70% strain, suggesting a colloidal transition beyond this threshold. Dynamic amplitude assessments were also carried out to examine the hydrogels' self-healing ability. Fig. 1I illustrates the application of a significant 400% strain amplitude aimed at disrupting the hydrogel network, succeeded by a minimal 1% strain to evaluate the recovery efficiency of the SIP. At 400% strain, the G' demonstrated a smaller

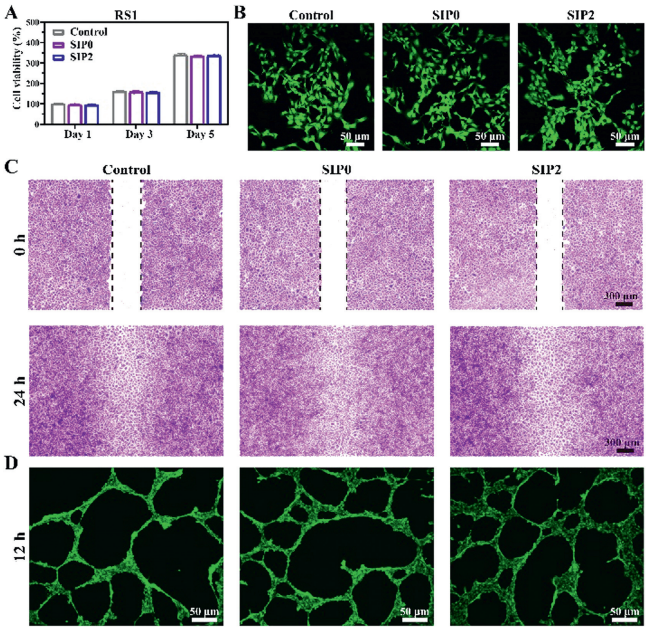

Fig. 2. Cellular *in vitro* studies conducted on SIP hydrogels. Examination of SIP hydrogels' cytotoxic effects on RS1 macrophages, utilizing CCK-8 (A) and calcein-AM/PI (B) methods (scale bar: 50 μm). (C) Tracking HUVEC cell migration over 0 and 24 h post-scratch assay (scale bar: 300 μm). (D) Images showing vascular formation in HUVECs treated with various samples (scale bar: 50 μm). Error bars denote the mean ± SD ($n = 3$).

reduction compared to the G'', hinting at hydrogel fracturing [27]. However, when the strain was reduced back to 1%, both moduli returned to their original states, indicating the hydrogel's rapid self-recovery. This cyclical deterioration and restoration process highlighted the hydrogel's exceptional self-healing qualities [28,29].

Thereafter, we evaluated the hydrogel dressings' swelling and deswelling behavior. The swelling curves in Fig. 1J revealed that both SIP0 and SIP2 hydrogels exhibited comparable water absorption dynamics. An initial rapid swell was observed in the first 5 min, subsequently leading to a slow attainment of equilibrium over 240 min. At equilibrium, SIP0 showed a water absorption rate of 16.86%, marginally surpassing SIP2's 15.41%. This suggests that IL-PBA incorporation improves hydrogel cross-linking. Regarding their capacity to retain water, the hydrogels underwent drying in a 37 °C environment until reaching a stable weight. In these circumstances, as demonstrated in Fig. 1K, SIP2 was superior to SIP0 in water retention. The gathered data affirm that the developed SIP hydrogels have remarkable abilities for water absorption and retention, beneficial for quickly soaking up wound exudate while maintaining a conducive moisture level for wound healing [30].

For the utilization of hydrogels as multifunctional dressings in tissue engineering and wound care, ensuring biosafety is crucial [31,32]. Initially, a concise evaluation of the biosafety at varying concentrations of IL-PBA was conducted. It was observed that cell viability remained above 85% when concentrations were between 0 and 600 μg/mL. However, as the concentration increased, a corresponding decline in cell viability was noted (Fig. S1 in Supporting information). Based on these findings, a concentration of 600 μg/mL was chosen as the upper limit for IL-PBA in our experiments. Next, our evaluation focused on the cytocompatibility of the developed SIP hydrogels, as shown in Figs. 2A and B. To assess cell viability, the cell counting kit-8 (CCK-8) method was employed following the co-cultivation of RS1 cell macrophages with SIP leachate over periods of 1, 3, and 5 days. Fig. 2A illustrates that the cell viability in both the SIP0 and SIP2 surpassed 80%, indicating low toxicity in the SIP hydrogels. After a 3-day culture period, the RS1 cells underwent staining with a calcein-AM/propidium iodide (PI) kit. Calcein-AM stained living cells green, while dead cells were marked red by PI [11]. The SIP hydrogel group exhibited green fluorescence at levels comparable to the control group, with scarcely any dead cells observed in the SIP hydrogel group, as evident in Fig. 2B.

After that, the SIP hydrogels' hemocompatibility was evaluated through a hemolysis assay. Fig. S2 (Supporting information) shows that the positive control group with DDW medium displayed a vivid red hue, signifying substantial rupture of red blood cells and hemoglobin release. Conversely, the groups containing phosphate buffered saline (PBS) and SIP hydrogels showed no color alteration, suggesting minimal hemolysis. The hemolysis rates for these groups stayed below 5%, reflecting superior hemocompatibility. The results indicate the SIP hydrogel's biocompatibility, with no hemolysis occurrence.

Subsequently, cell scratch tests were utilized to assess the influence of SIP hydrogels on cellular migratory characteristics (Fig. 2C) [9]. Human umbilical vein endothelial cells (HUVEC) cells were placed in a plate whose bottom was then scratched using a pipette tip. Following this, hydrogels were introduced, and variations in the scratched region were observed at 24 h of incubation. In the control group, cells exhibited typical migration and proliferation patterns with increasing culture time, markedly diminishing the traversed distance post 24 h (Fig. 2C). Comparatively, SIP hydrogels exhibited migration rates similar to those of the control group (Fig. S3 in Supporting information), suggesting that the synthesized hydrogel did not impair HUVEC cells' migration efficiency.

Moreover, HUVEC cells were used to assess the effects of the newly created SIP hydrogels on angiogenesis, as depicted in Fig. 2D. These cells were distributed over Matrigel and incubated. Our observations revealed that they started forming either polygonal or circular structures on Matrigel's surface. After prolonging the culture period to 12 h, HUVEC cells in the control set connected, creating a tubular network featuring an increased number of blood vessels and enhanced structural integrity [4]. In contrast, cells in the SIP hydrogel group remained closely packed and were able to develop a tubular network, suggesting that the SIP hydrogels effectively preserved the angiogenic capability of HUVCE cells.

Infections frequently interfere with the full recovery of wounds [11]. Our research explores a novel method for combating bacterial infections in diabetic wounds by incorporating active groups into a SerMA hydrogel matrix. This matrix is designed to trap bacteria using phenylboronic acid and destroy them with imidazole. Initially, SEM was employed to examine the efficiency of bacterial entrapment in SIP hydrogels (Fig. 3A). The findings demonstrated a significant enhancement in bacterial entrapment correlating with increased IL-PBA levels, especially in SIP0 (pure SerMA), SIP1 (with 0.3% IL-PBA), and SIP2 (with 0.6% IL-PBA).

Subsequently, the antibacterial effectiveness of the SIP hydrogels was assessed (Fig. 3B). A statistical evaluation indicated a 4.96% decrease in MRSA for the SIP0 hydrogel group and an impressive 68.06% reduction for the SIP1 group, whereas in the SIP2 group, MRSA was nearly entirely eradicated (Fig. S4 in Supporting information). Following this, a live/dead bacterial staining test was conducted to examine the anti-MRSA mechanisms of SIP hydrogels. Similar to the control group, the SIP0 group exhibited minimal red fluorescence, signifying an absence of bactericidal activity. In stark contrast, the SIP2 group showed intense red fluorescence, attributed to the penetration of propidium iodide through damaged bacterial membranes, causing a red tint in the bacteria [33]. Further statistical analysis revealed bacterial survival rates of 37.62% and 0% for the SIP1 and SIP2 groups (Figs. S5 and S6 in Supporting information), respectively, relative to the control.

To confirm the antibacterial effectiveness of SIP hydrogels, the structure of MRSA trapped within the hydrogels was scrutinized

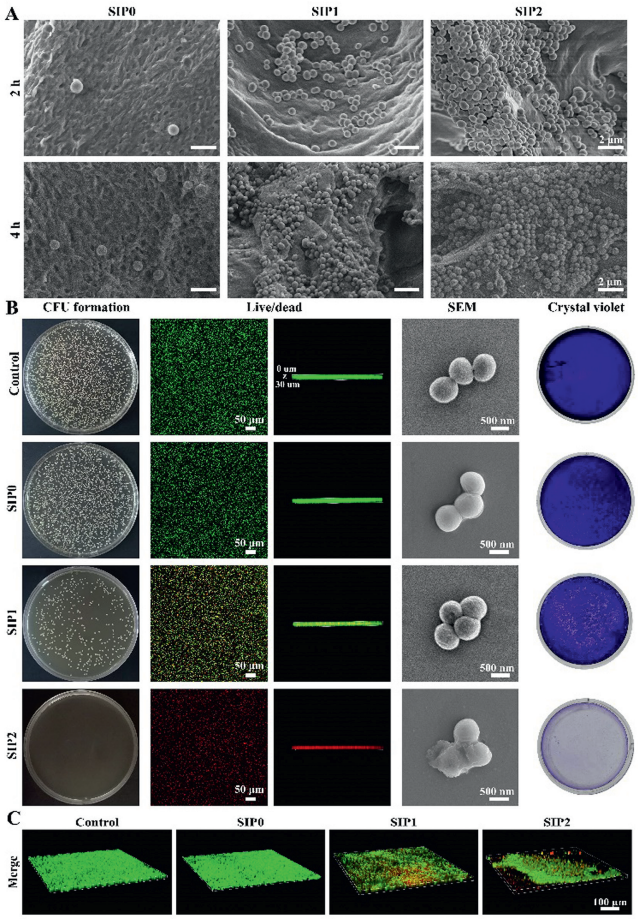

Fig. 3. Evaluation of SIP hydrogels' antibacterial effects. (A) Demonstrating SIP hydrogels' ability to capture MRSA, depicted through SEM images showing bacterial capture at 2 and 4 h (scale bar: 2 μm). (B) Investigating the anti-MRSA efficacy of SIP hydrogels using methods including agar plate analysis, live/dead staining (scale bar: 50 μm), SEM (scale bar: 500 nm), and crystal violet staining. (C) Illustration of SIP hydrogels disrupting established MRSA biofilms, shown through 3D live/dead bacterial imagery (scale bar: 100 μm).

using SEM. SEM images depicted a densely packed MRSA population on the SIP0, with no significant changes in bacterial surface structure. In contrast, the SIP1 hydrogel, while not greatly reducing MRSA numbers, showed significant wrinkling of the bacterial cell walls and membranes. With the SIP2 hydrogel, there was a discernible decrease in MRSA levels, along with extensive damage to the cell walls and membranes of many bacteria. This damage is likely due to the electrostatic attraction of the positively charged hydrogel, impacting bacterial membrane potential and hindering metabolic functions. In summary, the SIP2 hydrogel exhibits considerable effectiveness against MRSA, making it a promising candidate for wound dressing applications.

Furthermore, the crystal violet staining method was utilized to assess MRSA biofilm formation under various conditions. These methods yielded results similar to those observed for MRSA biofilms, where the SIP2 hydrogel significantly disrupted the biofilm structure. Further statistical examination showed a reduction in MRSA biofilm mass to 29.19% (Fig. S7 in Supporting information).

Next, investigations using three-dimensional (3D) confocal laser scanning microscopy (CLSM) yielded consistent results. Fig. 3C shows that the SIP2 hydrogel led to a reduction in biofilm build-up, likely due to the biofilm being disrupted by the hydrogel's three-dimensional structure. The SIP2 hydrogel, on the other hand, exhibited a substantial inhibitory effect, resulting in a notably sparse and fragmented biofilm. There was a marked decrease in biofilm signal intensity with higher IL-PBA content in the SIP hydrogels. This suggests that incorporating both capturing and killing agents into the SerMA matrix significantly enhances the system's ability to combat biofilm. In summary, the SIP2 hydrogel stands out as an effective solution for preventing biofilm formation.

Previous *in vitro* tests confirmed that SIP hydrogels possess excellent physicochemical properties, antimicrobial capabilities, and biocompatibility, making them suitable for treating bacteria-infected wounds. We then tested the wound healing efficacy of SIP hydrogel using a rat model. The SIPs' bleeding control was first examined using a rat tail amputation and a liver hemorrhage model. Fig. S8 (Supporting information) illustrates significant bleeding in the control group and the liver section covered in gauze, while the application of SIP2 hydrogel noticeably reduced blood loss. The blood loss amounts for the PBS, gauze, and SIP2 groups were 209, 146.67, and 41.67 mg, respectively (Fig. S8). Similar results emerged from the rat tail amputation test, where the SIP2 group showed considerably less bleeding than both the control and the gauze-covered tail. Blood loss measurements were 156.67, 128, and 32.67 mg for the PBS, gauze, and SIP2 groups, respectively (Fig. S9 in Supporting information). In conclusion, the SIP2 hydrogel shows a substantial hemostatic effect, promising for the therapy of chronic skin wounds.

Full-thickness skin defect models of diabetic rats were established to test the effect of each material on wound healing. Animal experiments have been approved by the Institutional Animal Care and Use Committee's regulations and guidelines at Wenzhou Medical University (approval number Wydw7019–0134). Evaluation of the healing effectiveness of the developed SIP hydrogel commenced with dorsal skin wounds in diabetic rats, depicted in Fig. 4A. PBS was used for treating the control group, whereas the positive control group underwent treatment with 3M hydrogel. SIP0 and SIP2 hydrogels were applied to the experimental groups. Wound healing progress was meticulously recorded and photographed on the 0, 3rd, 7th, and 14th days following treatment (Fig. S10 in Supporting information). Notably, within just three days, both the SIP0 and SIP2 groups showed a significant decrease in wound size compared to the PBS and 3M hydrogel groups. After one week, the SIP2 group demonstrated a remarkable reduction in wound size to just 19.34%, outperforming the other groups (Fig. S11 in Supporting information). By the 14th day, the PBS and 3M groups still exhibited larger wound areas, with 33.18% and 25.2% of the wounds remaining, respectively. The SIP0 group showed improved wound healing, decreasing the wound area to only 21.28%. Most impressively, the SIP2 group achieved the greatest healing success, reducing the wound area to a mere 10.69%. Bacterial samples were also collected from the wound sites and quantified through an agar plate method, as shown in Fig. S12 (Supporting information). Aligning with previous results, visible bacterial colonies were present in both the PBS and 3M groups. Conversely, such colonies showed a reduction in the SIP0 group and were nearly absent in the SIP2 group.

Fourteen days post-surgery, both wounds and nearby skin tissues underwent collection for histological examination, offering an enhanced understanding of the hydrogel's role in healing. Hematoxylin-eosin staining (H&E) staining showed that wounds treated with SIP2 displayed a fully restored epidermis and densely formed granulation tissue (Fig. 4C) [34]. In contrast, crust formation and infiltration by inflammatory cells were evident in both the PBS and 3M groups. Collagen fibers in the SIP2 group, as revealed by Masson's staining, were aligned parallel to hair follicles, indicating highly organized and uniform collagen deposition (Fig. 4D) [8]. Partially mature granulation tissue and an incomplete epidermal layer characterized wounds treated solely with SIP0. Furthermore,

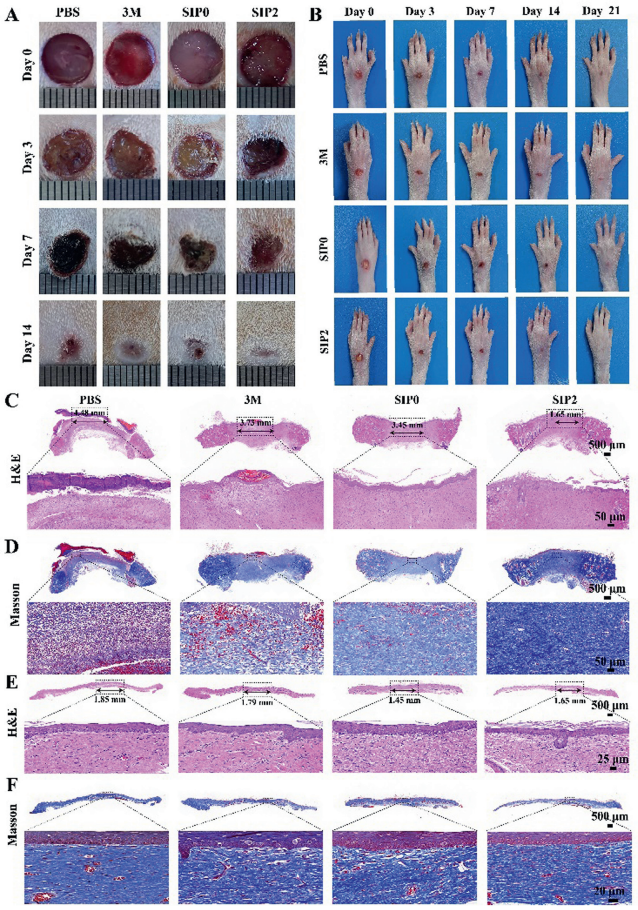

Fig. 4. Assessment of rat dorsal skin and DFU wound healing treated with SIP hydrogels. (A) Photographs of skin wounds in PBS, 3M, SIP0, and SIP2 groups, taken on days 0, 3, 7, and 14. (B) Photographic documentation of skin wounds treated with PBS, 3M, SIP0, and SIP2 at days 0, 3, 7, 14 and 21. Microscopic analysis of rat skin tissues in wounded regions using H&E (C), Masson (D) stains (scale bar: 50 μm). (E, F) Microscopic analysis of rat skin tissues at DFU wound locations using H&E (E, scale bar: 25 μm) and Masson (F, scale bar: 20 μm) stains.

the wound sites underwent evaluation for tumor necrosis factor-alpha (TNF-α) levels, a key cytokine in immune response (Fig. S13 in Supporting information) [35]. The PBS group exhibited the highest TNF-α levels, whereas the 3M, SIP0, and SIP2 groups had progressively lower levels, indicating reduced inflammation (Fig. S14 in Supporting information). Next, CD31 staining, used to identify vascular endothelial cells, indicated minimal CD31 expression in the PBS group [36]. In contrast, higher expression was observed in the SIP0 group and the highest in the SIP2 group, suggesting increased angiogenesis in the regenerating tissue (Figs. S13–S15 in Supporting information).

We then directed our attention to assessing the healing impact of the developed SIP hydrogel on DFUs in diabetic rats. For the study, a 5 mm diameter circular skin lesion was created on the rat's foot back using a biopsy punch (Fig. 4B). Various materials, each with a weight of 50 mg, were applied to these wound sites. Throughout the treatment, the progression of DFUs' healing was monitored and recorded through photographs on days 3, 7, 14, and 21. As shown in Fig. S16 (Supporting information), varying healing speeds were observed across different treatment groups. Rats receiving SIP0 and SIP2 hydrogel treatments exhibited quicker healing compared to those treated with PBS or 3M hydrogels, as shown in Fig. S17 (Supporting information). Significantly, at one week post-treatment, wounds treated with 3M continued to exhibit substantial open regions (accounting for 31.46% of the original wound size), similar to the PBS group (44.23% of the original size). This underscored the limited effectiveness of 3M hydrogel in promoting healing in the presence of bacterial infection. However, the wounds in the SIP0 group had significantly reduced, showing a 13.83% reduction in size by the 21st day, indicating the hydrogel's potential for expedited healing. Impressively, the SIP2 group exhibited almost complete wound closure by day 21, with only an average of 5.44% of the original wound size remaining unhealed. Additionally, bacterial samples were collected from the wound areas and quantified utilizing an agar plate method (Fig. S18 in Supporting information). In line with our previous observations, the PBS and 3M groups exhibited noticeable bacterial colonies. However, these colonies were less prevalent in the SIP0 group and virtually absent in the SIP2 group.

Twenty-one days after surgery, both the wounds and adjacent tissues were removed for histological examination aimed at further assessing the hydrogel's influence on wound healing. H&E staining (Fig. 4E) showed that wounds treated with SIP2 exhibited more complete healing, characterized by dense granulation tissue and a fully restored epidermis [37]. Contrastingly, groups treated with PBS and 3M exhibited crust formation and the presence of infiltrating inflammatory cells. The SIP groups' granulation tissue appeared less mature, and the epidermis was incompletely formed. Collagen, vital for cell growth, differentiation, and wound healing, was also examined [38]. Masson staining (Fig. 4F) indicated that collagen fibers in the SIP2 group aligned neatly and consistently parallel to the hair follicles [39]. Besides, the PBS group showed the highest TNF-α expression. Conversely, a progressive decline in TNF-α expression was observed in the 3M, SIP0, and SIP2 groups, indicating that the SIP2 treatment reduced inflammation in the wound (Figs. S18–S20 in Supporting information). Furthermore, in the negative control group, CD31 expression was faint, whereas it was more pronounced in the SIP0-treated group and strongest in the SIP2 group at the wound site, suggesting increased angiogenesis in the regenerated skin tissues (Figs. S18–S21 in Supporting information) [40]. This evidence implies that the SIP0 hydrogel, particularly when combined with IL-PBA, can promote epithelial regeneration and reduce inflammation, offering a novel approach to diabetic wound treatment.

In the final analysis, our specifically engineered SIP hydrogel dressings underwent a biosafety evaluation. Fig. S22 (Supporting information) reveals that, in rats treated with these dressings compared to the control group, there were no considerable changes across all measured parameters, indicating unaffected kidney and liver functionality. Moreover, examination of the key organs in rats from each group disclosed no notable pathological anomalies or damage (Fig. S23 in Supporting information) [23]. The gathered data reliably confirm the outstanding biological safety of SIP hydrogels, highlighting their significant promise for clinical application.

In summary, we have effectively engineered and constructed a cutting-edge antibacterial platform named SIP, particularly aimed at curing wounds in diabetics suffering from MRSA infections. Initially, we synthesized phenylboronic acid with double bonds to capture bacteria effectively and utilized imidazole for their elimination. These components were seamlessly integrated into a Sermatrix using a straightforward one-pot hybrid copolymerization process. Functionally, the SIP hydrogel dressing has proven to be extremely efficient in both capturing and killing bacteria, proving itself as a broad-spectrum, eco-friendly, and highly effective antibacterial treatment. Notably, the SIP platform showcased an impressive eradication rate against MRSA (99.5%) *in vitro* settings, as well as demonstrating strong bactericidal effects in animal models. This pioneering research provides valuable insights for the development of hydrogel wound dressings, marking a significant breakthrough in the domain of protein-based material sciences for antibacterial applications.

Declaration of competing interest

The authors declare that they have no known competing financial interests or personal relationships that could have appeared to influence the work reported in this paper.

CRediT authorship contribution statement

Jiajia Wang: Investigation. **XinXin Ge:** Methodology. **Yajing Xiang:** Investigation. **Xiaoliang Qi:** Writing – review & editing. **Ying Li:** Software. **Hangbin Xu:** Software. **Erya Cai:** Investigation. **Chaofan Zhang:** Investigation. **Yulong Lan:** Software. **Xiaojing Chen:** Resources. **Yizuo Shi:** Software. **Zhangping Li:** Supervision. **Jianliang Shen:** Validation.

Acknowledgment

The work was supported by the National Natural Science Foundation of China (No. 82372551).

Supplementary materials

Supplementary material associated with this article can be found, in the online version, at doi:10.1016/j.cclet.2024.109819.

References

[1] Y. Xiang, X. Qi, E. Cai, et al., Chem. Eng. J. 460 (2023) 141852.
[2] J.W. Song, H. Ryu, W. Bai, et al., Sci. Adv. 9 (2023) eade4687.
[3] S. Matoori, A. Veves, D.J. Mooney, Sci. Transl. Med. 13 (2021) eabe4839.
[4] P. Li, Q. Liu, M. Pei, et al., Chin. Chem. Lett. 35 (2024) 109457.
[5] A. Sharma, D. Sharma, F. Zhao, Adv. Healthc. Mater. 12 (2023) 2300556.
[6] L. Zhang, C. Hu, M. Sun, et al., Adv. Sci. 10 (2023) 2300328.
[7] M. Chang, T.T. Nguyen, Acc. Chem. Res. 54 (2021) 1080–1093.
[8] Y. Zhang, C. Xue, Y. Zhang, et al., Chin. Chem. Lett. 35 (2024) 109196.
[9] P. Xin, S. Han, J. Huang, et al., Chin. Chem. Lett. 34 (2023) 108125.
[10] X. Fan, F. Wang, X. Zhou, et al., Int. J. Nanomedicine 15 (2020) 10321–10330.
[11] S. You, Y. Xiang, X. Qi, et al., Mater. Today. Adv. 15 (2022) 100271.
[12] Y. Wang, C. Zhang, H. Zhang, et al., Chin. Chem. Lett. 33 (2022) 4605–4609.
[13] D. Pranantyo, C.K. Yeo, Y. Wu, et al., Nat. Commun. 15 (2024) 954.
[14] C. Xie, J. Luo, Y. Luo, et al., ACS Appl. Mater. Interfaces 15 (2023) 42329–42340.
[15] S. Cheng, H. Wang, X. Pan, et al., ACS Appl. Mater. Interfaces 14 (2022) 11144–11155.
[16] X. Fan, X. Wu, F. Yang, et al., Angew. Chem. Int. Ed. 61 (2022) e202113833.
[17] T.Y. Wang, X.Y. Zhu, F.G. Wu, Bioact. Mater. 23 (2023) 129–155.
[18] C. Cai, T. Wang, X. Han, et al., Chin. Chem. Lett. 33 (2022) 1963–1969.
[19] J. Zhao, N. He, J. Mater. Chem. B 8 (2020) 10474–10486.
[20] T. Wang, G. Qu, C. Wang, et al., Langmuir 35 (2019) 13999–14006.
[21] Q. Zeng, X. Qi, G. Shi, et al., ACS Nano 16 (2022) 1708–1733.
[22] M. Zhang, Y. Huang, W. Pan, et al., Carbohydr. Polym. 253 (2021) 117213.
[23] S. Yan, J. Li, Y. Gao, et al., ACS Appl. Mater. Interfaces 15 (2023) 48952–48962.
[24] L. Wang, L. Chen, J. Wang, et al., Chin. Chem. Lett. 33 (2022) 1956–1962.
[25] G. Liu, Y. Zhou, Z. Xu, et al., Chin. Chem. Lett. 34 (2023) 107705.
[26] Q. Zeng, Y. Qian, Y. Huang, et al., Bioact. Mater. 6 (2021) 2647–2657.
[27] X. Qi, Y. Xiang, E. Cai, et al., Chem. Eng. J. 439 (2022) 135691.
[28] X. Qi, X. Tong, S. You, et al., ACS Macro. Lett. 11 (2022) 861–867.
[29] U.S. Malik, Q. Duan, M.B.K. Niazi, et al., Chin. Chem. Lett. 34 (2023) 108071.
[30] X. Qi, E. Cai, Y. Xiang, et al., Adv. Mater. 35 (2023) 2306632.
[31] F. Liu, L. Wang, X. Zhai, et al., Carbohydr. Polym. 322 (2023) 121344.
[32] W. Pan, X. Qi, Y. Xiang, et al., Int. J. Biol. Macromol. 195 (2022) 190–197.
[33] C. Yang, X. Ma, P. Wu, et al., Small 19 (2023) 2301092.
[34] Q. Zhao, G. Qing, J. Yu, et al., Chin. Chem. Lett. 35 (2024) 108535.
[35] Z.Y. Li, X.J. Zhang, Y.M. Gao, et al., Adv. Healthc. Mater. 12 (2023) 2202770.
[36] X. Qi, Y. Huang, S. You, et al., Adv. Sci. 9 (2022) 2106015.
[37] S. Cheng, M. Pan, D. Hu, et al., Chin. Chem. Lett. 34 (2023) 108276.
[38] Y. Zong, B. Zong, R. Zha, et al., Adv. Healthc. Mater. 12 (2023) 2300431.
[39] L. Wu, Y. Chen, G. Zeng, et al., Chem. Eng. J. 457 (2023) 141244.
[40] Q. Bai, C. Zheng, N. Sun, et al., Acta Biomater. 154 (2022) 231–243.